University Library

MINERVA ACCESS

A gateway to Melbourne's research publications

Minerva Access is the Institutional Repository of The University of Melbourne

Author/s:
Masoomi-Godarzi, S;Hall, CR;Zhang, B;Gregory, MA;White, JM;Wong, WWH;Ghiggino, KP;Smith, TA;Jones, DJ

Title:
Competitive Triplet Formation and Recombination in Crystalline Films of Perylenediimide Derivatives: Implications for Singlet Fission

Date:
2020-05-28

Citation:
Masoomi-Godarzi, S., Hall, C. R., Zhang, B., Gregory, M. A., White, J. M., Wong, W. W. H., Ghiggino, K. P., Smith, T. A. & Jones, D. J. (2020). Competitive Triplet Formation and Recombination in Crystalline Films of Perylenediimide Derivatives: Implications for Singlet Fission. Journal of Physical Chemistry C, 124 (21), pp.11574-11585. https://doi.org/10.1021/acs.jpcc.0c01337.

Persistent Link:
https://hdl.handle.net/11343/344901

Competitive triplet formation and recombination in crystalline films of perylenediimide derivatives: implications for singlet fission

Saghar Masoomi-Godarzi[a,b], Christopher R. Hall[b], Bolong Zhang[a,b], Valerie D. Mitchell[a,b], Mark A. Gregory[a,b], Jonathan M. White[a,b], Wallace W. H. Wong[a,b], Kenneth P. Ghiggino[b], Trevor A. Smith[b] and David J. Jones[a,b]*

[a] Bio21 Institute and [b] School of Chemistry, University of Melbourne, Parkville, Victoria 3010, Australia.

*Corresponding author: djjones@unimelb.edu.au

Abstract

Singlet fission (SF) has become a highly active area of research due to its potential to increase the photoconversion efficiency limit. However, developing photostable compounds that undergo quantitative SF remains a key challenge. As singlet fission necessitates electron transfer between neighboring molecules, the SF rate is highly sensitive to intermolecular coupling and molecular orientation in the solid state. In this report, we investigate singlet fission in thin films for a series of perylenediimide (PDI) molecules that have favorable light harvesting properties including photostability and large molar extinction coefficients. By adding different substituents at the imide positions, the packing of the molecules in the solid state can be changed. The relationship between SF parameters and the stacked geometry in PDI films is investigated, with two-electron direct coupling found to be the main SF mechanism. Time-resolved emission and transient absorption (TA) data show that all of the PDI films undergo SF although with different rates and yields varying from 35 to 200%. The results show that PDI1 and 2, which are stacked PDI pairs twisted out of alignment along the HOMO to LUMO transition, exhibit faster and more efficient SF up to 200% yield. We demonstrate that both triplet formation and decay rates are highly sensitive to the ordering of the molecules within a film. The results of this study will assist the design of optimized structures with the large SF rate and low recombination rate that are required for useful light harvesting applications.

Key words: Singlet fission, perylenediimide, crystalline film, intermolecular interaction

1. Introduction

Singlet fission (SF) is a photophysical process that occurs in coupled organic molecules where the first singlet state has at least twice the energy of the corresponding triplet state i.e. $E(S_1) \geq 2 \times E(T_1)$. In this energetic configuration SF can generate two triplet excitons on absorption of a single high energy photon, and thereby has the potential to increase the theoretical photoconversion efficiency limit of photovoltaic (PV) devices from 32% to 46% and mitigate thermalization losses.[1-3] SF was first reported in anthracene crystals half a century ago, and has been reported since then with high yields in polyacenes,[4-5] such as tetracene, pentacene and their derivatives, oligophenyls,[6] diphenylisobenzofuran,[7] carotenoids,[8-9] rylene-based chromophores,[10] perylenediimides,[11] diketopyrrolopyrroles derivatives and conjugated polymers.[12-13] However, most of our understanding of the SF process relies on the experimental and computational work on the acene family. Perylenediimides (PDIs), in contrast to the acenes, have many properties that make them suitable for light harvesting applications.[14] They are photostable, resistant to photooxidation, have low production costs and display large molar extinction coefficients in the range of $5\text{-}10 \times 10^4$ M^{-1} cm^{-1} in the visible region.[15-19] They also meet the energy level requirement for SF with reported triplet energy levels around 1.1 eV, suggesting PDIs as ideal chromophores for SF-based light harvesting applications.[15-16, 20]

Theoretical calculations demonstrate two distinct pathways for the formation of triplets through singlet fission. The first is a two-step, one electron mechanism where a charge transfer (CT) state acts as an intermediate species for the triplet formation.[21] These CT states can be real or virtual intermediates. It has been reported that this CT-mediated mechanism can efficiently support SF where the energy of the CT state is low and the different intermolecular coupling is sufficiently large.[22-23] The other mechanism is a one-step, two electron mechanism that does not involve any intermediate states.[21, 24-26] Calculations for PDI molecules show that the energy of the CT state is about 4.5 eV using a Weller-like relation, which is about 2 eV above the S_1 energy level.[25] Despite the large values of V_{LL} and V_{LH}, which are the electronic couplings between S_1S_0 and the CT state and the CT state and T_1T_1, respectively, the energy of the CT state is too large for the indirect mechanism to play a role during SF. Also, PDI molecules in thin films and molecular crystals tend to pack closely in cofacial arrangements with an interplanar distance of about 3.5 Å, which

induces significant orbital overlap between neighboring molecules. This in turn produces strong charge resonance interactions that can facilitate one step, two electron exchange between neighboring molecules.[14]

Several studies have shown that the rate of SF is highly sensitive to the intermolecular coupling and even minor variations in the relative position of chromophores in a solid can make a significant change in the efficiency of the SF process.[25, 27] As a result, it is necessary to develop rules for favorable orientation of the coupled chromophores. For this purpose, various numerical calculations have been performed on the pairs of chromophores in the crystal using a simplified model with some assumptions and approximations to calculate the SF rate. These assumptions can cause errors and make the calculations unreliable and at variance with the experimental findings.[28] In addition, it has been found that for a prediction of desirable packing patterns in crystalline solids, it is necessary to consider the geometrical arrangements of a larger number of molecules simultaneously.[29] The better alternative to define these rules more accurately is making the crystal pairs by crystal engineering or by preparation of covalent dimers and comparing their SF behavior. PDI derivatives form well-ordered, π-stacked structures with a packing geometry that can be tuned by functionalizing the PDIs with different substituents. When the PDIs are functionalized at their imide positions, the functional groups have little impact on the electronic properties of the molecule compared to other positions.[30] However, in crystals, the functional groups allow control over the relative orientation of neighboring molecules, providing a mechanism for control over the intermolecular interactions.

In this paper, we map the relationship between various crystal pairs of PDI derivatives and the efficiency of the one step direct mechanism of SF. For this purpose, the ability of four PDI derivatives (Scheme 1) to undergo SF was studied. All four PDI derivatives (PDI1-4) are based on the same PDI core but are substituted differently at their imide positions; PDI1 by butylbenzene, PDI2 by butyl-terphenyl, PDI3 by diisopropylbenzene and PDI4 by mesitylene.

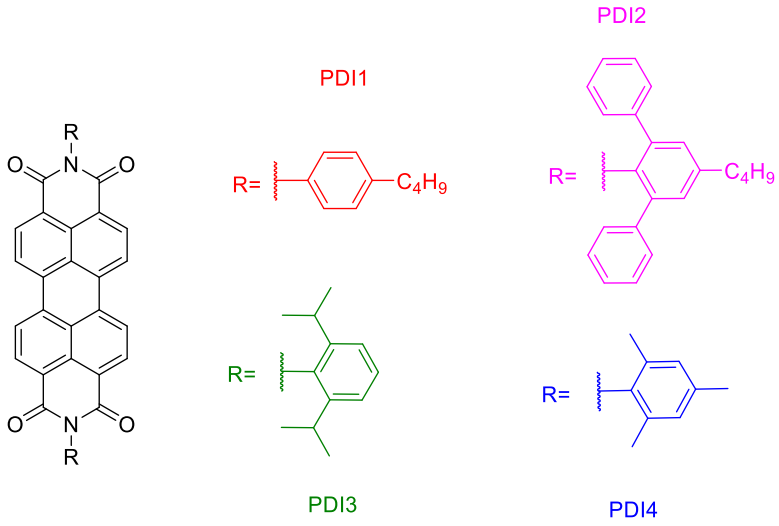

Scheme 1. The structures of the selected four PDI derivatives

Calculations show that as we progress from a perfectly stacked pair arrangement, which is unfavorable for SF, and slip one chromophore along the direction of the HOMO-LUMO transition moment, fast SF results. The effect of slipping distance on the efficiency of singlet fission has been investigated using models based on Marcus[10, 25] or Redfield[23, 28] theories in the slip-stacked pairs. Both models predict a large variation in SF rates as one chromophore is slipped with respect to its neighbor in their long and short axes. However, the two models predict different chromophore pair geometries that maximize SF efficiency. To the best of our knowledge, the effect of rotating one chromophore with respect to its neighbor around one of its axes in the crystal motif has not been investigated, either experimentally or theoretically, and this is one objective of this study. The other important factor for inclusion of SF materials in photovoltaic devices is the triplet lifetime of the SF material. The triplet should last long enough for charge extraction. We have investigated the triplet lifetime for all four PDI derivatives.

In this work, thin films of the four PDIs (1-4) have been evaluated with respect to their ability to support SF, using ultrafast transient absorption, flash photolysis and time-resolved fluorescence techniques to map the relationship between stacking geometry and SF parameters in a direct SF mechanism. Our results show that both triplet formation and decay rates are highly sensitive to the ordering of the molecules within a film. This study will help guide the design of an ideal geometry with a fast SF rate and low recombination rate, which is essential for light harvesting

applications. Also, we demonstrate a fast and efficient SF process in the PDI pairs when the direct two electron mechanism is dominant.

2. Experimental Methods

Material synthesis

The synthesis procedures of PDIs (1-4) have been reported elsewhere.[31-33] Palladium octabutoxyphthalocyanine ($PdPc(OBu)_8$) was synthesized following the literature procedure as described in the supplementary information (SI).[34] All chemicals were used as received from suppliers.

Film preparation

Glass substrates with dimensions of 2.5 cm × 2.5 cm were cleaned by sonicating sequentially in acetone, isopropanol and chloroform. Before thin film casting, the substrates were dried with a strong flow of nitrogen. Solutions of PDIs were prepared by dissolving the samples into chloroform at a concentration of 5 mg/mL. To prepare blend films for sensitized experiments, solutions of PDI mixed with $PdPc(OBu)_8$ were prepared by dissolving PDI and $PdPc(OBu)_8$ with mass ratio of 50:50 in chloroform at 5 mg/mL. Finally, thin films were cast onto clean glass substrates via spin coating at 1000 rpm/s and spun for 1 min. The crystalline film was prepared by solvent vapor annealing (SVA) of the film whereby chloroform was injected into a 30 mm glass Petri dish. The Petri dish was closed for 1 min to let the vapor saturate the treatment chamber. Then as-cast films were attached on the backside of the Petri dish lid, which was quickly swapped with the lid covering the solvent-containing Petri dish. The film was about 1 cm above the solvent level during the SVA. The optimal duration of SVA treatment used in this study was 60 s.[35]

Crystal structure determination

Single-crystals of PDIs were grown by slow diffusion of methanol or isopropanol vapor into the solution of chloroform. The single-crystal X-ray data for PDI3 were collected at 100 K on the MX1 beamline at the Australian Synchrotron. [36] The structures of PDI1 and PDI4 were collected at 100K on a Rigaku Synergy diffractometer. The structures were solved by direct methods and difference

Fourier synthesis. Thermal ellipsoid plots were generated using the program ORTEP-3 integrated within the WINGX suite of programs. The crystal data for PDI2 were published in our previous report. [31] Structures for PDI1, PDI3 and PDI4 have been deposited at the CSD and assigned CCDC deposit codes are 1949528, 1958260 and 1958261, respectively.

Thin film characterization

Samples for grazing incidence wide angle X-ray scattering transmission measurements were prepared by loading the materials onto silicon wafers. The samples were analyzed at the SAXS/WAXS beamline at the Australian Synchrotron with an X-ray energy of 10 keV.[37] A Pilatus 200K detector was used for wide-angle measurements. The substrates were silicon wafers that had been sonicated in acetone and isopropanol for 30 min each followed by 30 min of UV/ozone treatment. The beamline has a range of incident angles from Ω= 0.02−0.35 in 0.005 increments to allow signal optimization near the critical angle of the film but below the critical angle of the substrate. Data from GIWAXS experiments were analyzed using a customized version of NIKA 2D using IgorPro.[38-39]

Steady state spectroscopy

Absorption spectra were recorded for PDI derivatives using a Varian Cary 50 UV−vis spectrophotometer. Fluorescence spectra were recorded on a Varian Eclipse spectrofluorimeter using an excitation wavelength of 550 nm and excitation and emission bandwidths of 5 nm for solution and 10 nm for film measurements. Photoluminescence (PL) spectra in the near-IR region were recorded with a spectrometer (Horiba Jobin Yvon iHR320) and an amplified InGaAs photo-detector (Electro-Optical System). The excitation source was a supercontinuum laser (NKT Photonics, SuperK Extreme& Varia) for excitation wavelengths tunable across the 450-750 nm region. The excitation beam was mechanically chopped and the detector output was fed into a lock-in amplifier synchronized to the chopper frequency. A 750 nm high pass filter was used to remove the second order of the excitation and fluorescence. PL experiments at cryogenic temperatures were carried out in a liquid nitrogen cryostat (Oxford Instruments, Optistat DN).

Time correlated single photon counting

As described previously,[31] the excitation source was a mode-locked and cavity dumped Ti:Sapphire laser (Coherent Mira 900F/APE PulseSwitch) pumped by a Coherent Verdi-10 DPSS Nd:YVO_4 laser. The laser output (880 nm wavelength, 5.4 MHz repetition rate) was frequency doubled to provide an excitation wavelength of 440 nm. The individual fluorescence decay curves were collected using a time-correlated single photon counting (TCSPC) module (SPC-150, Becker & Hickl, Berlin, Germany). The fluorescence decay times were extracted from the decay profiles using FAST software (Edinburgh Instruments Ltd) and a sum-of-exponentials analysis.

Sub-nanosecond transient absorption spectroscopy

A mode-locked Ti:sapphire oscillator (Coherent, Mira Seed) seeded a Ti:sapphire regenerative amplifier system (Coherent, RegA 9050) to produce pulses of about 50 fs duration at a repetition rate of 92 kHz and a wavelength centered at 800 nm. A portion of the light was used to generate the 400 nm pump beam using a β-BBO (β-barium borate) crystal, and the 630 and 730 nm pump beams were generated with an optical parametric amplifier (OPA9450, Coherent). The pump beam was mechanically chopped at ~3.5 kHz, and the arrival time of the pump pulses relative to the probe was manipulated using a variable optical delay line (Newport, UTS150PP with ESP 300 controller). The broadband probe was derived from the residual 800 nm beam focused onto a 3 mm sapphire substrate (Crystal Systems) for measurements in the visible region (450−800 nm) and a 5 mm undoped YAG substrate (Crystal Systems) for the infrared region (800−1400 nm). After passing through the sample, the probe beam was analyzed with a CMOS detector (Ultrafast Systems) at 7077 spectra/s, and the excess 800 nm laser fundamental was blocked using low- and high-pass filters for the visible and IR regions, respectively. The relative orientation of the pump and probe polarization was 54.7° and all spectra were corrected for the chirp of the supercontinuum probe. Dry nitrogen was blown over films during all measurements.[40]

Flash photolysis

Flash photolysis was employed to monitor the triplet excited state lifetime. The measurements were conducted on a home built transient-absorption apparatus. The 5 ns duration pump pulses are generated by a Nd:YAG laser/OPO (Ekspla NL120, 10 Hz repetition rate), centered at 550 nm. For the probe we use a pulsed white light LED (Thorlabs, MCWHLP1) synchronized to the laser

pump source. The trigger pulse timing and duration are controlled with a BNC (Model 7010) delay generator and BK Precision 4064 waveform generator. The electronic trigger pulse train is connected to the modulation input of the Thorlabs LED controller (DC2200). The pump and probe beams are focused to 0.5 cm FWHM spot at the sample position. After the sample, the probe beam is collimated and re-focused onto the entrance slit of a spectrometer (SpectraPro-300i, Acton Research Corporation, 0.3 meter spectrograph, 150 l/mm grating blazed at 500 nm). A photomultiplier tube (1P28, Hamamatsu) detected the spectrometer output at a given probe wavelength. The PMT analogue voltage is acquired with a digitizing oscilloscope (Teledyne LeCroy WaveSurfer 10). The signal kinetics were analyzed using FLASH software (Edinburgh Instruments Ltd).

Global target analysis

To study the mechanism from a large transient absorption data set, advanced modeling and data analysis techniques such as global and target analysis are needed to derive models and decompose spectra into their overlapping component spectra. Specifically, Global Target Analysis (GTA) is an approach based on differential equations that is employed to analyze multidimensional data sets for kinetic modeling and spectral interpretation. In this study, the program Glotaran[41] was used for the analysis. This approach starts with a simple model with a defined number of components and a set of starting values for the rate constants describing the kinetic connectivity between the components. The whole transient absorption data set is fit by generating the time dependent population evolution of spectral intensities from a set of first order differential equations. Then, the parameters are optimized by re-adjusting the starting values based on the resulting model. The quality of the fit can be judged from the fitted spectra and time traces as well as residual matrices. Any residual structure in the singular vectors displays a potential misfit and the need for another component in the proposed model. After checking and accepting the fitted model, the program generates kinetic traces, the evolution of populations and spectra of each component. GTA was used to separate the overlapping features and generate the population profiles for each component versus time.

3. Results

Structural characterization

All four PDI derivatives (PDI1-4) are based on the same core but are substituted differently at their imide positions; PDI1 by butylbenzene, PDI2 by butyl-terphenyl, PDI3 by diisopropylbenzene and PDI4 by mesitylene (Scheme 1). This has a significant impact on their intermolecular interaction and crystal packing (Figure 1). The molecules of PDI1, 3 and 4 pack in the monoclinic crystal system in the $P2_1/c$, $P2_1/n$ and $P2_1$ space groups with one molecule in the unit cell whereas PDI2 packs in the triclinic crystal systems in the P1 space groups with two molecules in the unit cell. The crystallographic parameters of PDI1-4 are summarized in Table S1 in the supporting information.

In all four PDI molecules, the PDI core is roughly flat with dihedral angle, Θ_1, for the four carbons comprising the bay position as shown in Figure S1 ranging from 0.43° to 2.63°, which are listed in Table 1. In addition, the phenyl groups at the imide position are twisted by Θ_2 out of the PDI plane by 117° - 118°. The molecules PDI1 and 2 show herringbone packing with π-π overlap between neighboring molecules, whereas PDI3-4 packs in π-stacking columns in a lamellar arrangement (Figure 1). Dichlorobenzene molecules used as the solvent are trapped between PDI4 molecules in the lattice which will affect the PDI-PDI distance along the z axis (d_z) however the GIWAX patterns fit with this crystal structure. In order to investigate the intermolecular interaction for each PDI, the structures of the two nearest neighboring units from the crystal packing of the four PDI derivatives (PDI1-4) are shown in Figure 2. The PDI3 molecules form slip-stacked pairs with π-π stacking distances ($r_{\pi-\pi}$) of 5.2 Å and slipping distances of 6.3 Å in the x axis (Δx), and 1.2 Å in the y axis (Δy) (Figure 2c). PDI4 molecules also form slipped stacked dimers with the neighboring molecules slipped by 3.5 Å in the x axis (Δx), and no offset in the y axis (Δy) (Figure 2d). On the other hand, PDI1 and 2 form π-π stacked PDI pairs twisted out of alignment as shown in Figure 2a and b. These molecules show a different rotational angle against their neighboring chromophore through the xy plane, Θ_3, that is of about 90° and 45° for PDI2 and 1, respectively. The measured $r_{\pi-\pi}$ is 3.5 Å for PDI1 and 4.5 Å for PDI2. The values for $r_{\pi-\pi}$, Δx, Δy, Θ_1 and Θ_2 are summarized in Table 1. PDI3 has the largest $r_{\pi-\pi}$ and PDI1 displays the shortest $r_{\pi-\pi}$. PDI3 displays the least overlap between the neighboring chromophores compared to the other derivatives of

PDI, which leads to a weaker intermolecular interaction. PDI1, with a twist angle of 45° and the shortest π-π distance, has the strongest intermolecular interaction among the other derivatives.

Table 1. The structural parameters for the associated dimers of the four PDI derivatives including π-π stacking distance $r_{\pi-\pi}$, displacement distance along the x axis (Δx) and y axis (Δy), the dihedral angles of the four carbons (Θ_1), the torsion angle of phenyl (Θ_2) and rotation angle (Θ_3)

	$r_{\pi-\pi}$ (Å)	Δx (Å)	Δy (Å)	Θ_1 (degrees)	Θ_2 (degrees)	Θ_3 (degrees)
PDI1	3.5	-	-	1.26	117	45
PDI2	4.5	-	-	2.63	118	90
PDI3	5.2	6.3	1.2	0.43	117	-
PDI4	-	3.5	0	2.25	117	-

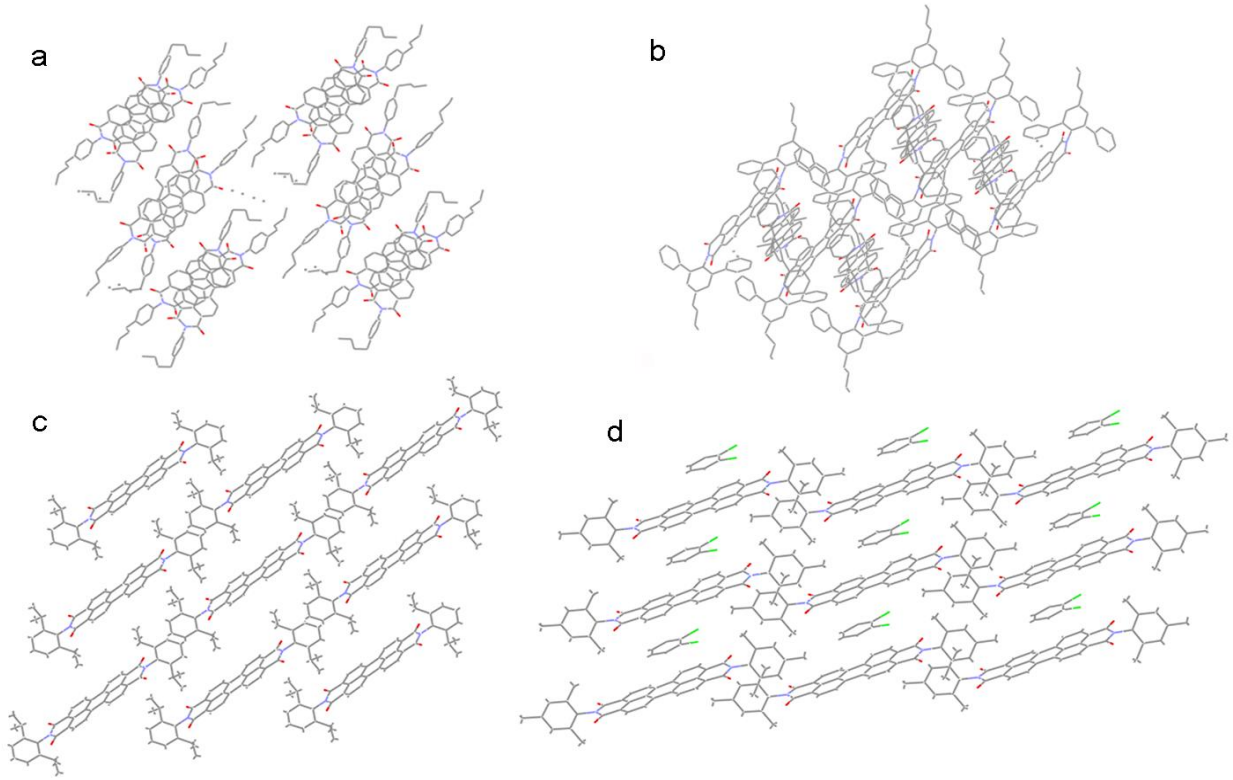

Figure 1. The lattice packing of (a) PDI1, (b) PDI2, (c) PDI3 and (d) PDI4.

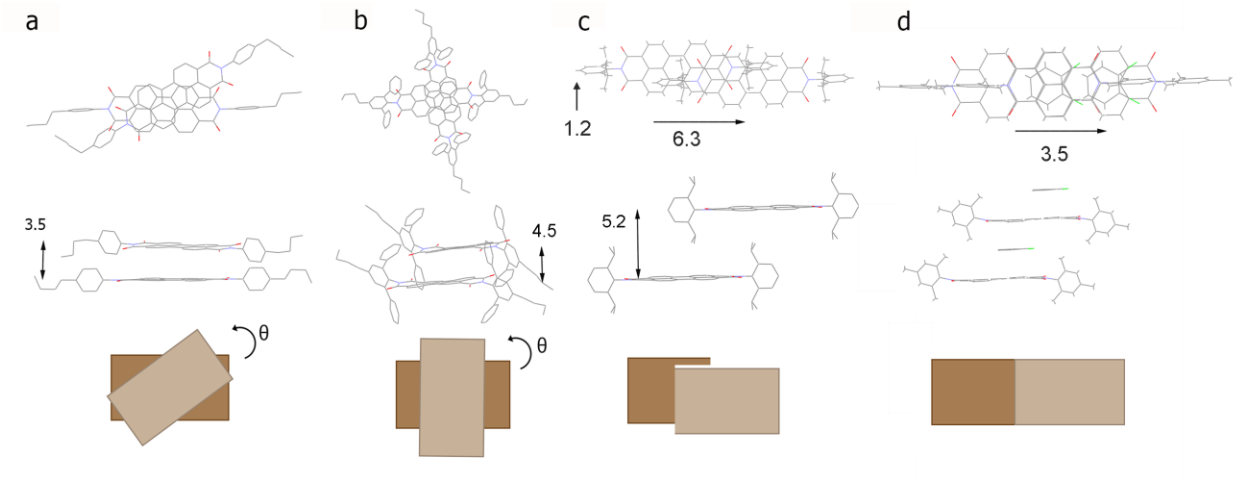

Figure 2. The associated pair units from the crystal packing of (a) PDI1, (b) PDI2, (c) PDI3 and (d) PDI4. Top view (upper row) and side view (middle row) and representation of the overlapping PDI arrangements (lower row). The distance units are in Å.

Thin film characterization

Grazing incidence wide-angle X-ray scattering (GIWAXS) measurements were performed on the as-cast and solvent vapor annealed (SVA) thin films of all PDI derivatives. The resulting scattering patterns of PDI1 and 3-4 are shown in Figure S2A-C. GIWAXS data contain information about the structural changes upon annealing and the results of the SVA film can be compared to the reported crystal structure for each PDI molecule. For PDI1, the scattering patterns for both the as-cast and SVA film indicate speckled rings suggesting long range crystalline order and the scattering rings in the as-cast film are more isotropic (Figure S2A1-2). The scattering pattern for PDI3 shows two closely spaced rings in the as-cast film which is indicative of a small amount of isotropic crystallinity and after annealing the crystallinity is increased dramatically indicating isotropic long range order (Figure S2B1-2). The scattering pattern indicates little or no crystalline order in the as-cast thin film of PDI4 with no significant peaks in the GIWAXS (Figure S2C1) indicating that the films are effectively amorphous. However, the PDI4 SVA film shows speckled rings and crystalline order (Figure S2C2). The PDI2 as-cast and SVA film shows no crystalline order with no peak detected in the GIWAXS. The results suggest that the crystallinity of the film is increased consistently by solvent vapor annealing the as-cast film. The in-plane and out-of-plane patterns for the SVA thin films from GIWAXS are compared to the corresponding powder patterns simulated from the single crystal structures and the linecuts are compared to find a preferred

orientation (Figure S3). For PDI1 and 3-4, the linecuts of GIWAXS spectra for the SVA film closely match with the reported single crystal structures.

Steady state optical properties

Figure 3A-D shows the solution and SVA thin film absorption and fluorescence spectra of the four PDI molecules (PDI1-4). For comparison, the corresponding spectra of the four PDI derivatives in as-cast thin films are also shown in Figure S4 in the Supplementary Information. The similarity of these spectra in solution suggests that the substitutions at the imide position have only minor effects on the photophysical properties of the PDIs in solution, but influence their solid state packing. For all of the studied PDI derivatives in solution, the fluorescence spectra mirror their absorption features and show small Stokes shifts. For all the PDI derivatives both the absorption and fluorescence spectra are different to one another in the solid state and compared to when in solution, which is attributed to different extents of intermolecular association. PDI1 in the film shows a broader and blue-shifted absorption band with loss of vibronic features compared to its monomeric form (assumed from the solution), features characteristic of H-type aggregation as mentioned in our previous report.[31] PDI2 and 3 in films show broader and slightly red-shifted absorption spectra (relative to the solution case) with similar or slightly smaller A_1/A_2 ratios (A_1 and A_2 are the main absorption peaks as illustrated in Figure 3), which is attributed to a mixture of H and J aggregates as mentioned in our previous report for PDI2.[31] PDI4 shows a slightly broader and red-shifted absorption spectrum with different A_1/A_2 ratio in the film compared to its monomer. Minor changes in the absorption and fluorescence spectra of the PDI derivatives are observed upon solvent vapor annealing (SVA) due to changes in the orientation and coupling of the chromophores in the more crystalline film induced by SVA, compared to the amorphous films. On the other hand, no change in the spectrum of PDI1 is observed upon SVA.

It was reported that both short-range charge transfer (CT) coupling and long range coulombic coupling are simultaneously present in the π-stacking molecules that are associated with the formation of H and J-aggregates.[42] Spano and coworkers demonstrated that the absorption spectra of PDI derivatives comprise features that result from competition between short and long range couplings. They showed how the relative sign and magnitude of these two interactions

affect the absorption spectrum by representing the total coupling between neighboring molecules as the sum of J_{coul}+J_{CT}. For PDI1, the broadening of the absorption spectrum and loss of vibronic features in the film relative to its monomer with a greatly attenuated A_1/A_2 ratio, are characteristics of H-aggregates where the sum of coulombic and CT-mediated coupling is positive (J_{coul}+J_{CT} >0). For PDI2 and 3, the solid-state absorption spectrum strongly resembles the monomer with a small red-shift, which is characteristic of a H/J null aggregate. This is due to the coulombic coupling being of opposite sign and similar magnitude as the CT-mediated coupling, so the sum is zero (J_{coul}+J_{CT} =0). For PDI4, the solid state absorption spectrum shows a red-shift and an increase in the A_1/A_2 ratio relative to the monomer, which is characteristic of J/H aggregates, so the sum of the coulomb and CT-mediated coupling is negative (J_{coul}+J_{CT} <0).

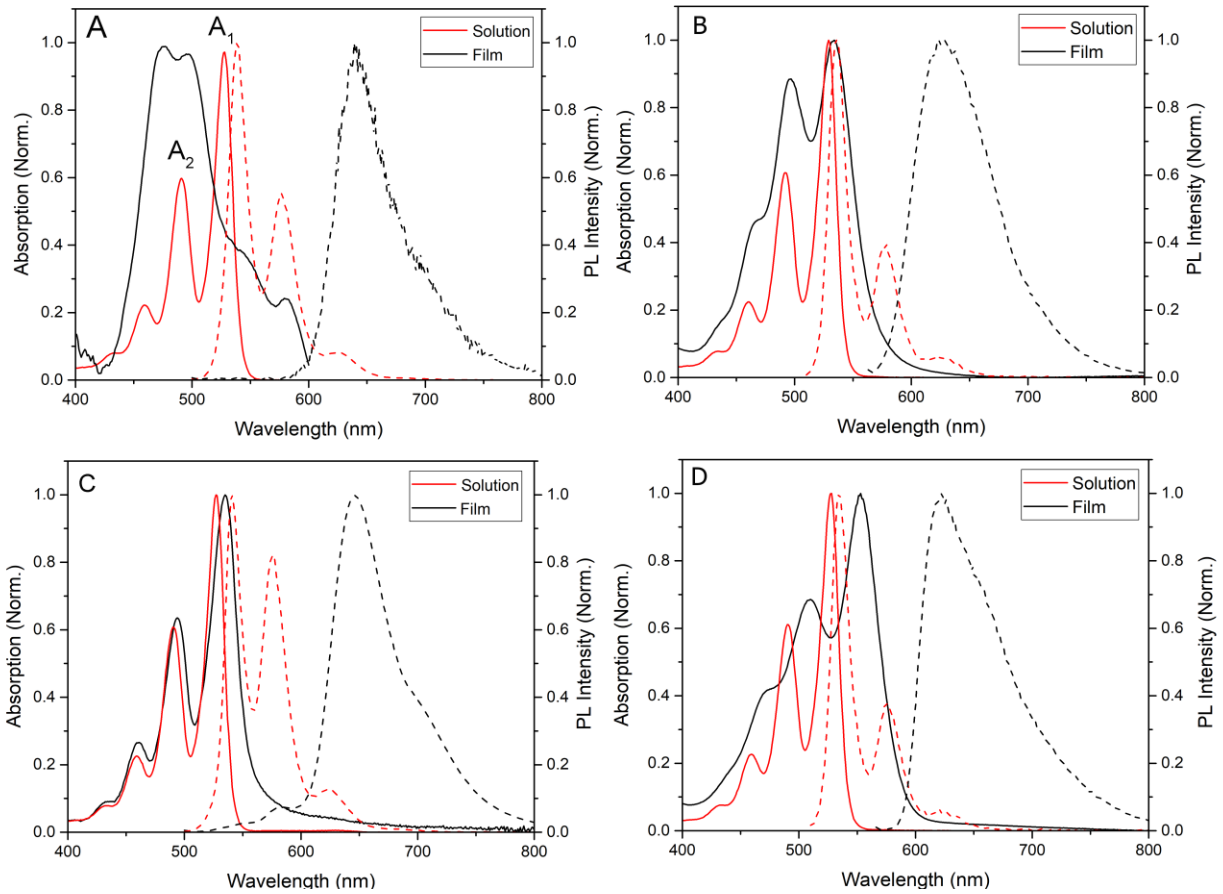

Figure 3. Steady state absorption (solid lines) and emission spectra (dashed lines) of dilute chloroform solutions (red) and SVA thin films (black) of (A) PDI1, (B) PDI2, (C) PDI3 and (D) PDI4.

Time-resolved photoluminescence of PDI derivatives

The fluorescence decay profiles, acquired by time correlated single photon counting (TCSPC) (see Figure S5), of PDI2-4 in SVA films show bi-exponential decay behavior upon excitation at 400 nm. The fluorescence of PDI1 was too weak to be measured at 650 nm. For PD2, PDI3 and PDI4 the shorter decay component has a time constant of 0.59, 0.27 and 0.22 ns while the longer second component has a time constant of 2.15, 2.02 and 1.7 ns, respectively. The fluorescence decay of the PDI4 SVA film is compared with the as-cast thin film and a dilute chloroform solution in Figure 4. The fluorescence decay of PDI4 in as-cast thin films decays (with time constants of τ_1=0.45 ns and τ_2=1.7 ns) faster than in solution (with decay time of 4.9 ns) indicating additional pathways are available to depopulate the excited state in the more condensed state of the film, possibly including excimer formation. In addition, the fluorescence decay of PDI4 in the annealed film differs from the as-cast film with decay times of τ_1=0.22 ns, τ_2=1.7 ns. The reduced value for τ_1 indicates an additional quenching pathway for fluorescence in the annealed film which is not present in the as-cast film, or the formation of different crystalline phases which exhibit different fluorescence decay characteristics to the more amorphous regions.

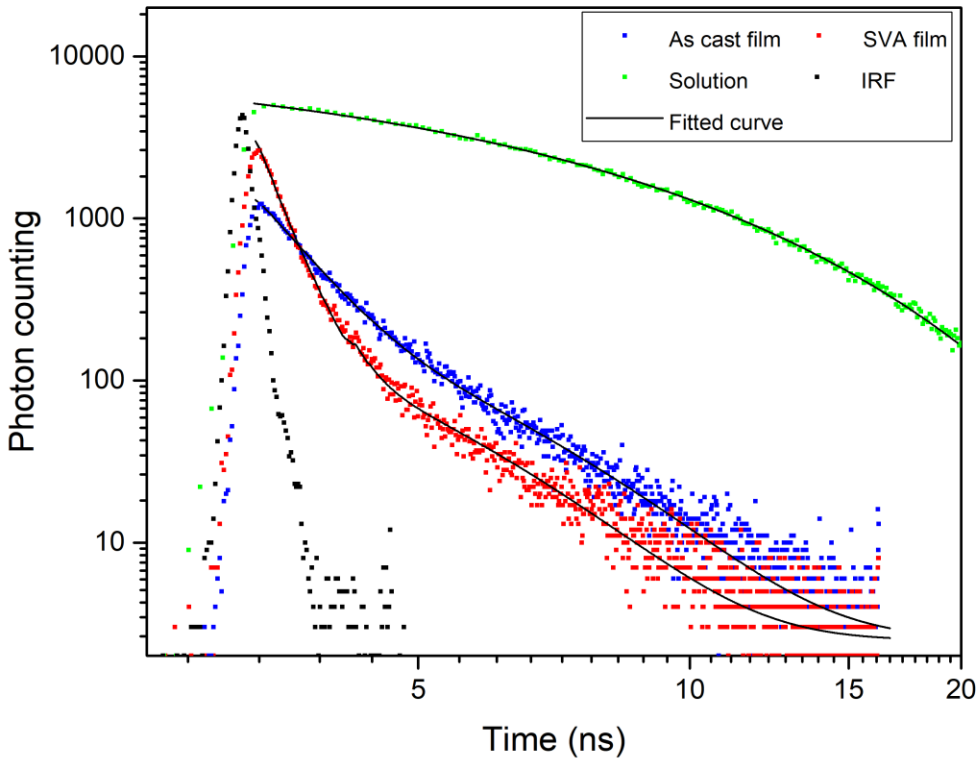

Figure 4. Fluorescence decay curves for SVA, as-cast film and dilute chloroform solution of PDI4 recorded by TCSPC at 650, 650 and 520 nm following excitation at 400 nm. The solid lines are the best fits using bi-, bi- and single exponential decay functions, respectively.

Ultrafast transient absorption spectroscopy

Ultrafast transient absorption spectroscopy (TA) was performed for PDI1-4 in chloroform solution, and the as-cast and SVA thin films. The samples were excited at 540 and 550 nm with low pump energy of 1 nJ/pulse and fluence of 10 $\mu J/cm^2$ to avoid singlet-singlet exciton annihilation. The TA spectra in the visible region at different time delays of 0 to 800 ps and kinetic traces at 580 and 700nm of PDI4 in solution are shown in Figure S6A and B, respectively. A ground state bleach (GSB, 450-650 nm) and a photoinduced absorption band (PIA1, > 650 nm) are apparent. The decay of the PIA1 band is concomitant with the ground state recovery (Figure S6B) and there is no sign of triplet formation. PDIs 1-3 also show the same kinetic and spectral behavior in dilute chloroform solution (data not shown).

The TA spectra and kinetic traces at 500 and 650 nm of PDI1-4 in as-cast films are shown in Figure 5 and S6, respectively. A GSB and a positive photoinduced absorption band (PIA1, beyond 550 nm) with similar but mirrored kinetics are observed for all PDI2-4 compounds and no sign of triplet formation is observed. PDI3 shows the fastest decay and PDI2 shows the slowest decay to the ground state. However, different excited state dynamics are seen in the SVA PDI films (Figure 6 and S7). Besides the GSB and PIA1 features, the evolution of a new positive absorption band stretching from 550 nm to 650 nm (PIA2) appears in the TA spectra of the SVA PDI2-4 films with the concomitant decay of the PIA1 (Figure 6). The kinetic traces at selected wavelengths for the SVA thin films of the PDI2-4 samples are shown in Figure S8. Comparison between Figures S6 and S7 shows the effect of annealing on the excited-state kinetics. In PDI2, the extracted kinetic traces at 500 and 670 nm corresponding to GSB and PIA1 consist of short and long-lived features in the SVA film (Figure S8A), whereas the as-cast film shows mono-exponential decay (Figure S7B). The extracted decay curve at 600 nm (PIA2) indicates a growth of PIA2 concomitant with the decay of PIA1. In PDI3 and 4, the kinetic traces in SVA films (Figure S8B-C) also show different kinetics from the as-cast films (Figure S7B-C) and the formation of a new feature. This suggests that the PDIs' singlet exciton decay follows the growth of another feature with different rates for each

PDI sample in SVA films. This is in agreement with time-resolved photoluminescence data which show exciton quenching in the SVA film which is not present in the as-cast film.

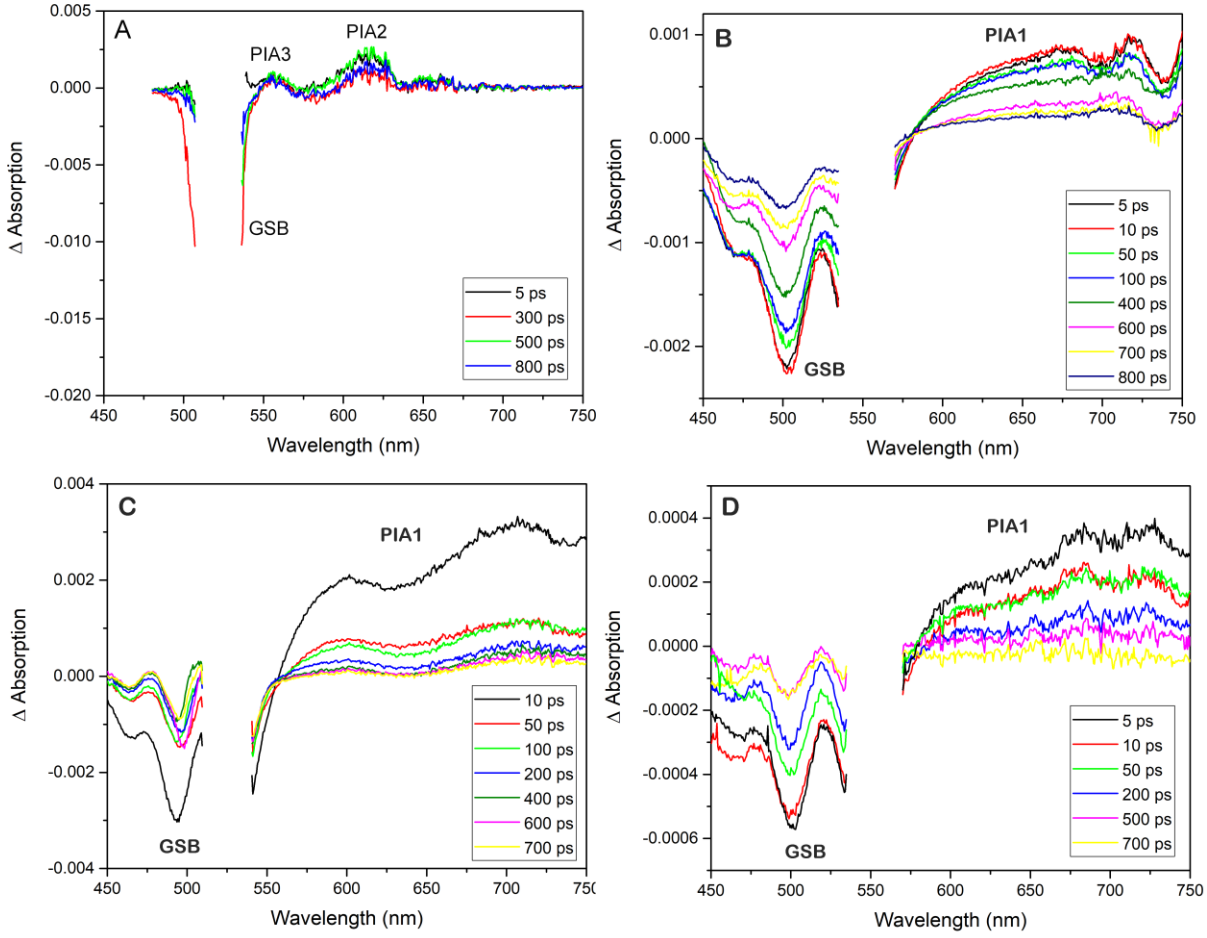

Figure 5. Transient absorption spectra of as-cast A) PDI1, B) PDI2, C) PDI3 and D) PDI4 films at different time delays in the range of 0-800 ps.

The TA spectra of PDI1 look different from the other three samples showing the formation of PIA2&3 at very early time delays and no PIA1 (singlet exciton) can be detected. This suggests that the singlet exciton decays quickly to another electronic state with absorption bands assigned PIA2&3 which could not be detected within the time resolution of this technique. Also, PDI1 shows the same dynamics in both as-cast and SVA films presumably due to the high crystallinity of the PDI1 sample in both films as confirmed from GIWAX data. Unfortunately, the high crystallinity and subsequent heterogeneous nature of PDI1 films causes a low signal to noise ratio and the kinetic data cannot be used.

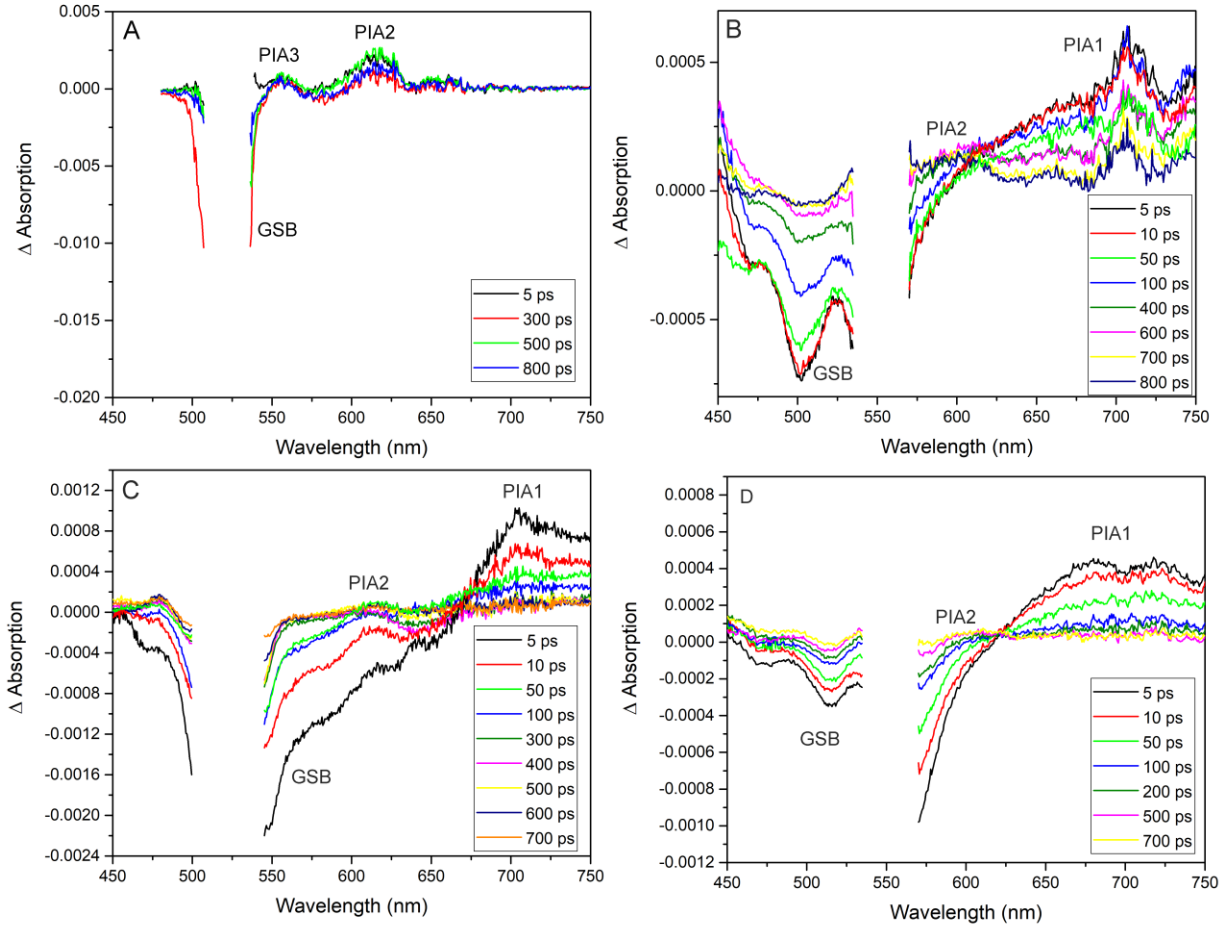

Figure 6. Transient absorption spectra of A) PDI1, B) PDI2, C) PDI3 and D) PDI4 in SVA films at different time delays in the range of 0-800 ps

The TA spectra and the kinetics of SVA PDI2-4 films were analyzed by singular value decomposition (SVD) and global target analysis (GTA) to identify the species associated spectra (Figure 7) and kinetic parameters (Table 2). The data were best fit by a two species sequential A → B→ GS model. The time constants that result from the fit ($k_1=1/\tau_1$) are summarized in Table 2. The first excited state decays with a time constant of k_1 to state B that is identical to the triplet absorption signal of PDI previously reported in the literature.[11, 14] This state then decays to the ground state. The assignment of the triplet absorption spectra will be discussed in the next section in more detail. From the global analysis, a direct conversion mechanism ($S_1 \rightarrow T_1$) shows the best fit to the TA data of all the PDI derivatives in SVA films suggesting that either no intermediate state is formed or it cannot be detected in this spectral region with the available

time resolution. The fast formation of triplets can be indicative of SF in the annealed PDI films. The results suggest that SF in SVA PDI films is highly sensitive to the intermolecular coupling and crystallinity of the films, since it is not observed in the amorphous films. The role of intermolecular coupling and its effect on SF parameters will be discussed in detail below.

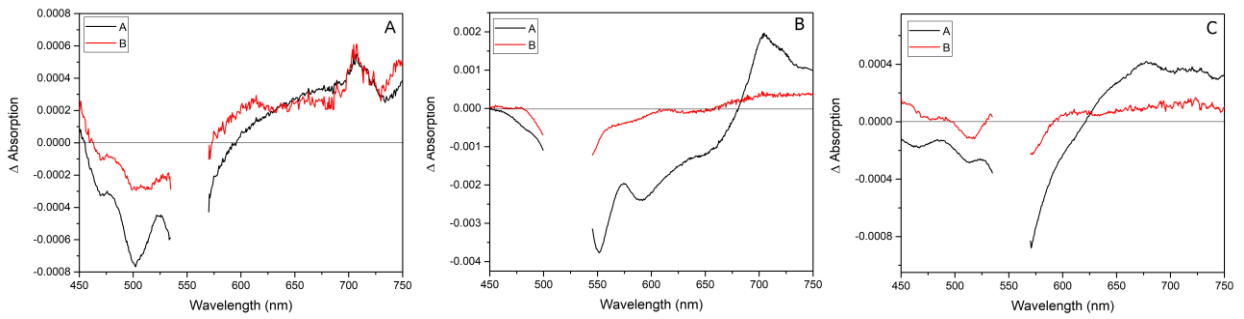

Figure 7. The species-associated spectra resulting from global target analysis of the TA data of SVA films of A) PDI2, B) PDI3 and C) PDI4. All data sets were fit using a two species sequential model.

Triplet Characterization

To obtain the triplet absorption spectrum of PDI and to prove that the species B in the TA spectra of the PDI SVA films is due to the triplets and not any other long-lived species, a triplet sensitization experiment was performed. $PdPc(OBu)_8$ was chosen as the triplet sensitizer because it undergoes rapid intersystem crossing and has two narrow absorption bands at 370 and 730 nm (Figure S9) which makes the direct excitation of PDI derivatives possible, and a triplet energy level of 1.1 eV (see Figure S10) that is higher than the PDI triplet energy level. The TA spectra of $PdPc(OBu)_8$ in a thin film excited at 730 nm, show a GSB at 650-750 nm and a PIA in the spectral region of 500-650 nm that decays to the ground state and is assigned to the triplet excited state (Figure S11). The transient absorption spectra of $PdPc(OBu)_8$:PDI4 are shown in Figure S12. Although $PdPc(OBu)_8$ was excited selectively, the GSB from PDI4 is observed in the spectral region of 480-560 nm showing triplet energy transfer takes place from $PdPc(OBu)_8$ to PDI4 so the photoinduced absorption peak at about 600 nm is due to the PDI4 triplet absorption which is consistent with the literature. To provide more information about the dynamics of the triplet decay in PDI4, laser flash photolysis measurements were performed on the $PdPc(OBu)_8$:PDI film.

The photoinduced absorption decay curve is shown in Figure S13, following excitation at 650 nm showing a bi-exponential decay with one time constant of 300 ns and slower time constant of 5.2 μs which might be due to the presence of $PdPc(OBu)_8$ triplet. The T_1-induced absorption peak obtained from the sensitization experiments is similar to the absorption spectrum of the 2nd species extracted from the GTA of the SVA PDI films. This confirms that the 2nd species (PIA2) in the SVA PDIs are triplets rather than any other long-lived state. As a result, we confirm that triplets are formed on an ultrafast time scale following excitation of the SVA PDI films, but are not observed in the as-cast films or solutions.

Flash photolysis spectroscopy of PDI films

The triplet decays in the SVA PDIs thin films were measured by laser flash photolysis. The GSB recoveries in both the as-cast and SVA films of PDI1-4 at 500 nm are shown in Figure 8A and B, following excitation at 550 nm. The weak GSB signal in PDI1 is due to the low quality and highly crystalline nature of the film. The GSB kinetics of the PDI2-4 as-cast films show single fast components with kinetics limited to the instrument response function (IRF). The annealed thin films of PDI2-4 and PDI1 show much slower kinetics, with bi-exponential character, fitting with fast time constants of 100, 95, 120 and 55 ns and slower time constants of 0.6, 0.8, 1.05 and 1.2 μs for PDI1-4, respectively. The sensitizer-generated isolated triplets are long-lived, of about 5 μs. PDI1 shows the fastest triplet decay and PDI4 the slowest triplet decay. The change in the dynamics of the GSB recovery in the PDI thin films upon annealing, in combination with the ultrafast TA results, suggest fast triplet formation via singlet fission following different triplet dynamics from the sensitized film. The two triplet lifetimes suggest that triplets decay with different rates in different crystalline regions in films of a given compound.[43] A faster recombination rate for the triplet pairs generated in PDI1-4 via SF is due to the enhanced contribution of spin-allowed geminate triplet-triplet annihilation. The fast triplet formation (~100 ps) in PDI1-4 suggests SF is the dominant process of triplet formation rather than intersystem crossing (ISC), because in most cases ISC on such a short timescale is only observed in systems with heavy atoms.[44]

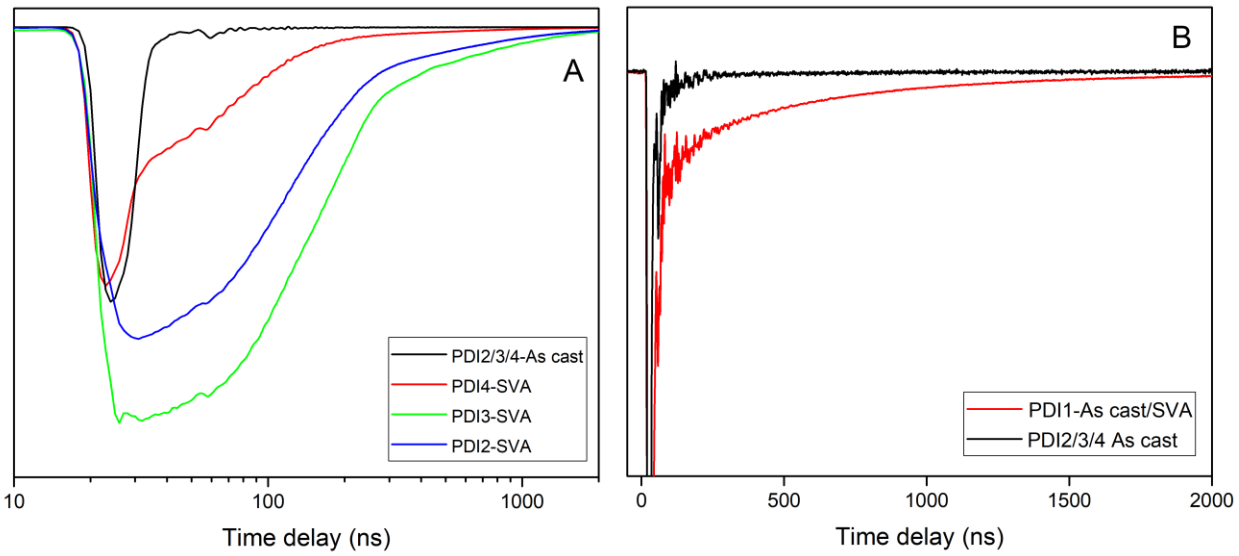

Figure 8. Ground state bleach recoveries of (A) SVA and as-cast thin films of PDI2-4 and (B) thin film of PDI1 and as-cast films of PDI2-4 monitored at 500 nm following excitation at 550 nm with excitation density of 30 μJ/cm^2.

Triplet yield calculation

In an ideal singlet fission chromophore, two triplets can be formed per absorbed photon. To determine the triplet yield, which is the main characteristic of SF, different methods are employed. One of the most reliable and accurate methods is the triplet sensitization technique in which a suitable triplet sensitizer undergoes energy transfer to the triplet states of the SF chromophore. In this method, the triplet extinction coefficient for the SF molecule is first determined using a triplet sensitizer with known triplet extinction coefficient. The number of triplets contributing to the triplet-triplet absorption band of the PDI SVA film are then quantified using the PDI triplet extinction coefficient. The excitation density of the sample is calculated and used to determine the number of singlet excitons generated during the experiments. Finally, the triplet yield is measured as the ratio of the number of triplets per singlet. The triplet extinction coefficient ($\Delta\varepsilon_{PDI}$) for the PDI4 thin film is measured to be $\Delta\varepsilon_{PDI}$= 3850 cm^{-1} M^{-1} at 600 nm (further details of this calculation are given in the Supplementary Information). To determine the concentration of singlet excitons, the excitation density of the sample is calculated using:

$$\xi = \frac{E\lambda K(1-10^{-A})}{la}$$

where E is the pump energy, λ is the pump wavelength, K= 5.034×10^{-15} J^{-1} nm^{-1}, A is the absorbance of the sample at the pump wavelength, *l* is the sample thickness and *a* is the spot size of the pump pulse. The excitation density then is used to calculate the percentage of molecules in the film that are excited and finally the concentration of singlet excitons that are formed is calculated. The triplet yield and lifetime from flash photolysis measurements and SF rate derived from the GTA are summarized in Table 2. The details of the triplet yield calculation are described in the Supplementary Information.

Table 2. Triplet yield, lifetime and SF rate of PDI1-4 SVA films

Sample Name	Triplet yield (%) ± 50%	Triplet lifetime		SF rate (ps^{-1})
		1^{st} rate constant (ns)	2^{nd} rate constant (μs)	
PDI1	200	100	0.6	> 0.1
PDI2	180	95	0.8	0.02
PDI3	35	120	1.05	0.004
PDI4	60	130	1.2	0.005

4. Discussion

We have studied singlet fission in four PDI molecules which pack differently in the thin film state. The molecules of PDI3 and 4 form slip-stacked pairs with their nearest neighboring chromophore, shown in Figure 2. PDI1 and 2 form π-π stacked PDI pairs twisted out of alignment with different rotational angle against their neighboring chromophore through the xy plane. The time-resolved emission, TA and flash photolysis data show that all of the PDI films undergo SF in SVA films although with different rates and yields. PDI1 and PDI2 show faster and more efficient SF compared to PDI3 and PDI4 suggesting that the chromophores with more orbital overlap between neighboring molecules and smaller π-π stacking distances ($r_{\pi-\pi}$) show faster SF. Marcus[10, 25] and Redfield[23, 28] demonstrated how the variation in SF rate of PDI pairs can be predicted with the change in the degree of slip displacement through the x and y axis in the packing arrangement of chromophores. However, unfortunately, there is no model available to predict the effect of rotating one chromophore with respect to its neighbor in one of its axes in the crystal motif on SF rate and it can be useful to have this information to correlate the experimental results with theory in the future. In this study, the energy of the CT state is too high

to be populated by the initial excited state as discussed in the previous section so two-electron direct coupling is the main mechanism for SF in these series of compounds. For SF by direct coupling, the intrinsic SF rate is proportional to the square of the Hamiltonian matrix element $<S_1S_0|H_{el}|T_1T_1>$. Michl et. al.[3] have calculated this matrix element as the difference between the two electron repulsion integrals of ($< l_A l_B|e^2/r_{12}|h_B l_A > \text{and} < h_A h_B|e^2/r_{12}|l_B h_A >$ (I_1 and I_2) where l_A, l_B, h_A and h_B are the LUMO and HOMO orbitals of two chromophores A and B. They demonstrated that if the stacking is perfect, there is as much attraction as there is repulsion, and two integrals (I_1 and I_2) cancel each other. However, if the stacked molecules are mutually shifted in the direction of the HOMO to LUMO transition moment, the cancellation is no longer perfect and the two integrals differ in sign, which results in a nonzero integral. The distribution patterns of the highest occupied molecular orbital (HOMO) and the lowest unoccupied molecular orbital (LUMO) are demonstrated in Figure S14. These suggest that the two PDI pairs of 1 and 2 that stacked in parallel planes slipped along the direction of the h→l transition, which is of importance for the fast SF and that might be the reason why PDI1 and 2 show faster and more efficient SF compared to the other compounds.

Once triplet pairs are formed via SF, they are coupled and can either decay to the ground state quickly or re-encounter each other and recombine to higher triplet or singlet excited states (K_{TTA1}). Also, they can diffuse apart before recombination and undergo slow non-radiative decay to the ground state (K_{TTA2}) which is an important step for device applications. The schematic diagram of energy levels and the kinetic model for SF dynamics of the PDI molecules are shown in Figure 9. The energy level of the first excited triplet state was reported previously (T_1=1.05 eV)[15-16, 20] and the higher triplet state is derived from TA measurements (T_2=3.05 eV, $\Delta T(T_2\text{-}T_1)$=2 eV, 620 nm). Triplet pairs that recombine can only form singlet excitons as triplet recombination to form higher energy triplet states is energetically forbidden. The kinetic decay of the triplet species also varies with the change in the packing arrangement of the chromophores in the film. PDI1 shows the shortest and PDI4 the longest-lived triplet states in the film suggesting that the chromophore with more orbital overlap with its neighboring molecules shows faster triplet recombination rates. It has been shown that the recombination rate of the triplets depends highly on the three-dimensional spatial diffusion of triplet excitons in the film.[45] Also, a high

binding energy can be another reason why triplet pairs cannot diffuse apart.[46] The results show that both triplet formation and decay rates are highly sensitive to the ordering of the molecules within a film and finding an ideal geometry with a fast SF rate and low recombination rate is still a challenge. One of the issues in employing SF chromophores in photovoltaic devices is the limited amount of time that the triplet excitons are available to be utilized for light harvesting applications. The ideal system for a SF capable photovoltaic application not only needs strongly coupled chromophore pairs to allow SF to occur but also needs weakly coupled chromophore pairs to allow triplet pairs to diffuse apart.

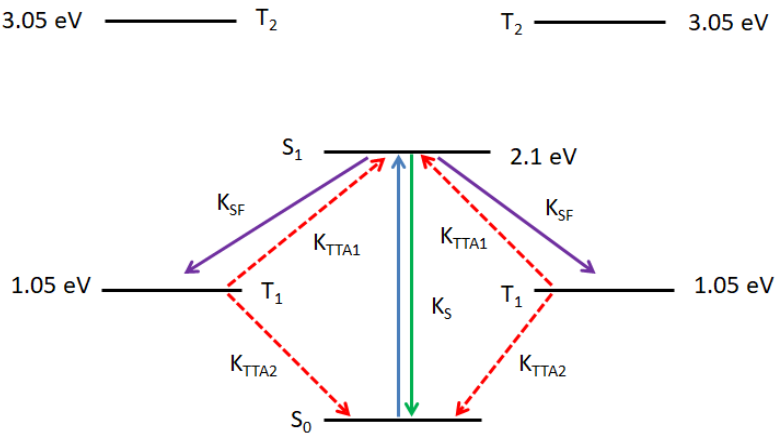

Figure 9. Schematic diagram of energy levels and the kinetic model for SF dynamics of PDI molecules

5. Conclusion

Due to their high stability, synthetic accessibility and high extinction coefficient, PDIs are potentially useful chromophores for SF-based applications. In this study, four PDI derivatives were investigated comprising the same PDI core but with different substituents at their imide positions, butylbenzene, butyl-terphenyl, diisopropylbenzene and mesitylene which display distinct molecular geometries with varied intermolecular π-π interactions. The ultrafast TA, time-resolved fluorescence and flash photolysis spectroscopies show that SF occurs with different rates and yields in SVA thin films of all the PDI derivatives but not in disordered PDI aggregates or in solution. By comparing structural information from single crystal diffraction, the triplet lifetime and SF rate and yield of each derivative can be related to intermolecular electronic coupling and orientations of the adjacent PDI chromophore. The X-ray crystal structures of the

PDI1-4 show that these chromophores are closely stacked in the solid state with π-π stacking distances of 3.5-5.2 Å and that PDI3 and 4 form slip-stacked pairs with their nearest neighboring chromophore. On the other hand, PDI1 and 2 form π-π stacked PDI pairs twisted out of alignment along the HOMO to LUMO transition. The ultrafast TA results demonstrate that PDI1 with more orbital overlap between neighboring molecules and smaller $r_{\pi-\pi}$, shows faster SF. The flash photolysis data show that PDI1 has the shortest and PDI4 the longest-lived triplet species in the films suggesting that the chromophore with more orbital overlap with its neighboring molecules shows the shorter-lived triplets, i.e. faster triplet recombination rate. This study affords a better understanding to identify the packing motifs that enhance SF efficiency in chromophores having two-electron direct coupling as the main SF mechanism. These results confirm that where there is a high SF yield, this comes with a shorter triplet lifetime, and therefore, a lower probability to potentially harvest the triplets. New approaches are required to find optimized geometries that will allow the generated triplets to be harvested effectively.

Acknowledgements

This work was made possible by support from the Australian Renewable Energy Agency which funds the project grants within the Australian Centre for Advanced Photovoltaics. This work was also supported by the ARC Centre of Excellence in Exciton Science (CE170100026). Responsibility for the views, information or advice expressed herein is not accepted by the Australian Government. We gratefully acknowledge the SAXS/WAXS beamline and beamtime via the Collaborative Access Program (proposal number 13618b) at the Australian Synchrotron.

References

1. Rao, A.; Friend, R. H., Harnessing Singlet Exciton Fission to Break the Shockley–Queisser Limit. *Nat. Rev. Mater.* **2017**, *2*, 17063-17075.
2. Shockley, W.; Queisser, H. J., Detailed Balance Limit of Efficiency of P-N Junction Solar Cells. *J. Appl. Phys.* **1961**, *32*, 510-519.
3. Smith, M. B.; Michl, J., Singlet Fission. *Chem. Rev.* **2010**, *110*, 6891-936.
4. Burdett, J. J.; Bardeen, C. J., Quantum Beats in Crystalline Tetracene Delayed Fluorescence Due to Triplet Pair Coherences Produced by Direct Singlet Fission. *J. Am. Chem. Soc.* **2012**, *134*, 8597-8607.
5. Geacintov, N.; Pope, M.; Vogel, F., Effect of Magnetic Field on the Fluorescence of Tetracene Crystals: Exciton Fission. *Phys. Rev. Lett.* **1969**, *22*, 593-596.

6. Zenz, C.; Cerullo, G.; Lanzani, G.; Graupner, W.; Meghdadi, F.; Leising, G.; De Silvestri, S., Ultrafast Photogeneration Mechanisms of Triplet States Inpara-Hexaphenyl. *Phys. Rev. B: Condens. Matter Mater. Phys.* **1999**, *59*, 14336-14341.
7. Akdag, A.; Wahab, A.; Beran, P.; Rulisek, L.; Dron, P. I.; Ludvik, J.; Michl, J., Covalent Dimers of 1,3-Diphenylisobenzofuran for Singlet Fission: Synthesis and Electrochemistry. *J. Org. Chem.* **2015**, *80*, 80-9.
8. Gradinaru, C. C.; Kennis, J. T. M.; Papagiannakis, E.; van Stokkum, I. H. M.; Cogdell, R. J.; Fleming, G. R.; Niederman, R. A.; van Grondelle, R., An Unusual Pathway of Excitation Energy Deactivation in Carotenoids: Singlet-to-Triplet Conversion on an Ultrafast Timescale in a Photosynthetic Antenna. *Proc. Natl. Acad. Sci.* **2001**, *98*, 2364-2369.
9. Wang, C.; Tauber, M. J., High-Yield Singlet Fission in a Zeaxanthin Aggregate Observed by Picosecond Resonance Raman Spectroscopy. *J. Am. Chem. Soc.* **2010**, *132*, 13988-13991.
10. Miller, C. E.; Wasielewski, M. R.; Schatz, G. C., Modeling Singlet Fission in Rylene and Diketopyrrolopyrrole Derivatives: The Role of the Charge Transfer State in Superexchange and Excimer Formation. *J. Phys. Chem. C.* **2017**, *121*, 10345-10350.
11. Le, A. K.; Bender, J. A.; Roberts, S. T., Slow Singlet Fission Observed in a Polycrystalline Perylenediimide Thin Film. *J. Phys. Chem. Lett.* **2016**, *7*, 4922-4928.
12. Mauck, C. M.; Hartnett, P. E.; Margulies, E. A.; Ma, L.; Miller, C. E.; Schatz, G. C.; Marks, T. J.; Wasielewski, M. R., Singlet Fission Via an Excimer-Like Intermediate in 3,6-Bis(Thiophen-2-Yl)Diketopyrrolopyrrole Derivatives. *J. Am. Chem. Soc.* **2016**, *138*, 11749-61.
13. Tavan, P.; Schulten, K., Electronic Excitations in Finite and Infinite Polyenes. *Phys. Rev. B: Condens. Matter Mater. Phys.* **1987**, *36*, 4337-4358.
14. Le, A. K.; Bender, J. A.; Arias, D. H.; Cotton, D. E.; Johnson, J. C.; Roberts, S. T., Singlet Fission Involves an Interplay between Energetic Driving Force and Electronic Coupling in Perylenediimide Films. *J. Am. Chem. Soc.* **2018**, *140*, 814-826.
15. Eaton, S. W., et al., Singlet Exciton Fission in Polycrystalline Thin Films of a Slip-Stacked Perylenediimide. *J. Am. Chem. Soc.* **2013**, *135*, 14701-14712.
16. Ford, W. E.; Kamat, P. V., Photochemistry of 3,4,9,10-Perylenetetracarboxylic Dianhydride Dyes. 3. Singlet and Triplet Excited-State Properties of the Bis(2,5-Di-Tert-Butylphenyl)Imide Derivative. *The Journal of Physical Chemistry* **1987**, *91*, 6373-6380.
17. Huang, C.; Barlow, S.; Marder, S. R., Perylene-3,4,9,10-Tetracarboxylic Acid Diimides: Synthesis, Physical Properties, and Use in Organic Electronics. *J. Org. Chem.* **2011**, *76*, 2386-2407.
18. Langhals, H.; Karolin, J.; B-Å. Johansson, L., Spectroscopic Properties of New and Convenient Standards for Measuring Fluorescence Quantum Yields. *J. Chem. Soc., Faraday Trans.* **1998**, *94*, 2919-2922.
19. Nakazono, S.; Easwaramoorthi, S.; Kim, D.; Shinokubo, H.; Osuka, A., Synthesis of Arylated Perylene Bisimides through C−H Bond Cleavage under Ruthenium Catalysis. *Org. Lett.* **2009**, *11*, 5426-5429.
20. Fukuzumi, S.; Ohkubo, K.; Ortiz, J.; Gutiérrez, A. M.; Fernández-Lázaro, F.; Sastre-Santos, Á., Control of Photoinduced Electron Transfer in Zinc Phthalocyanine−Perylenediimide Dyad and Triad by the Magnesium Ion. *J. Phys. Chem. A.* **2008**, *112*, 10744-10752.
21. Smith, M. B.; Michl, J., Recent Advances in Singlet Fission. *Annu. Rev. Phys. Chem.* **2013**, *64*, 361-86.
22. Berkelbach, T. C.; Hybertsen, M. S.; Reichman, D. R., Microscopic Theory of Singlet Exciton Fission. I. General Formulation. *J. Chem. Phys.* **2013**, *138*, 114102.
23. Mirjani, F.; Renaud, N.; Gorczak, N.; Grozema, F. C., Theoretical Investigation of Singlet Fission in Molecular Dimers: The Role of Charge Transfer States and Quantum Interference. *J. Phys. Chem. C.* **2014**, *118*, 14192-14199.

24. Havenith, R. W. A.; de Gier, H. D.; Broer, R., Explorative Computational Study of the Singlet Fission Process. *Mol. Phys.* **2012**, *110*, 2445-2454.
25. Renaud, N.; Sherratt, P. A.; Ratner, M. A., Mapping the Relation between Stacking Geometries and Singlet Fission Yield in a Class of Organic Crystals. *J. Phys. Chem. Lett.* **2013**, *4*, 1065-1069.
26. Zimmerman, P. M.; Bell, F.; Casanova, D.; Head-Gordon, M., Mechanism for Singlet Fission in Pentacene and Tetracene: From Single Exciton to Two Triplets. *J. Am. Chem. Soc.* **2011**, *133*, 19944-19952.
27. Wang, L.; Olivier, Y.; Prezhdo, O. V.; Beljonne, D., Maximizing Singlet Fission by Intermolecular Packing. *J. Phys. Chem. Lett.* **2014**, *5*, 3345-3353.
28. Havlas, Z.; Michl, J., Guidance for Mutual Disposition of Chromophores for Singlet Fission. *Isr. J. Chem.* **2016**, *56*, 96-106.
29. Buchanan, E. A.; Michl, J., Optimal Arrangements of 1,3-Diphenylisobenzofuran Molecule Pairs for Fast Singlet Fission. *Photochem. Photobiol. Sci.* **2019**, *18*, 2112-2124.
30. Delgado, M. C. R.; Kim, E.-G.; Filho, D. A. d. S.; Bredas, J.-L., Tuning the Charge-Transport Parameters of Perylene Diimide Single Crystals Via End and/or Core Functionalization: A Density Functional Theory Investigation. *J. Am. Chem. Soc.* **2010**, *132*, 3375-3387.
31. Zhang, B.; Soleimaninejad, H.; Jones, D. J.; White, J. M.; Ghiggino, K. P.; Smith, T. A.; Wong, W. W. H., Highly Fluorescent Molecularly Insulated Perylene Diimides: Effect of Concentration on Photophysical Properties. *Chem. Mat.* **2017**, *29*, 8395-8403.
32. Aksakal, N. E.; Chumakov, Y.; Yuksel, F., Crystal Structures of Two Perylenediimides: A Study of Bay-Substitution. *J. Chem. Crystallogr.* **2019**, *49*, 72-79.
33. Cao, P.; Khorev, O.; Devaux, A.; Sägesser, L.; Kunzmann, A.; Ecker, A.; Häner, R.; Brühwiler, D.; Calzaferri, G.; Belser, P., Supramolecular Organization of Dye Molecules in Zeolite L Channels: Synthesis, Properties, and Composite Materials. *Chem.: Eur. J.* **2016**, *22*, 4046-4060.
34. Soldatova, A. V.; Kim, J.; Rizzoli, C.; Kenney, M. E.; Rodgers, M. A. J.; Rosa, A.; Ricciardi, G., Near-Infrared-Emitting Phthalocyanines. A Combined Experimental and Density Functional Theory Study of the Structural, Optical, and Photophysical Properties of Pd(Ii) and Pt(Ii) A-Butoxyphthalocyanines. *Inorg. Chem.* **2011**, *50*, 1135-1149.
35. Sun, K., et al., A Molecular Nematic Liquid Crystalline Material for High-Performance Organic Photovoltaics. *Nat. Commun.* **2015**, *6*, 6013.
36. Cowieson, N. P., et al., Mx1: A Bending-Magnet Crystallography Beamline Serving Both Chemical and Macromolecular Crystallography Communities at the Australian Synchrotron. *J. Synchrotron Radiat.* **2015**, *22*, 187-190.
37. Kirby, N. M.; Mudie, S. T.; Hawley, A. M.; Cookson, D. J.; Mertens, H. D. T.; Cowieson, N.; Samardzic-Boban, V., A Low-Background-Intensity Focusing Small-Angle X-Ray Scattering Undulator Beamline. *J. Appl. Crystallogr.* **2013**, *46*, 1670-1680.
38. Gann, E.; Gao, X.; Di, C.-a.; McNeill, C. R., Phase Transitions and Anisotropic Thermal Expansion in High Mobility Core-Expanded Naphthalene Diimide Thin Film Transistors. *Adv. Funct. Mater.* **2014**, *24*, 7211-7220.
39. Ilavsky, J., Nika: Software for Two-Dimensional Data Reduction. *J. Appl. Crystallogr.* **2012**, *45*, 324-328.
40. Schwarz, K. N.; Geraghty, P. B.; Jones, D. J.; Smith, T. A.; Ghiggino, K. P., Suppressing Subnanosecond Bimolecular Charge Recombination in a High-Performance Organic Photovoltaic Material. *J. Phys. Chem. C.* **2016**, *120*, 24002-24010.
41. Snellenburg, J. J.; Laptenok, S.; Seger, R.; Mullen, K. M.; van Stokkum, I. H. M., Glotaran: A Java-Based Graphical User Interface for the R Package Timp. *J. Stat. Softw* **2012**, *49*, 22.
42. Manas, E. S.; Spano, F. C., Absorption and Spontaneous Emission in Aggregates of Conjugated Polymers. *J. Chem. Phys.* **1998**, *109*, 8087-8101.

43. Roberts, S. T.; McAnally, R. E.; Mastron, J. N.; Webber, D. H.; Whited, M. T.; Brutchey, R. L.; Thompson, M. E.; Bradforth, S. E., Efficient Singlet Fission Discovered in a Disordered Acene Film. *J. Am. Chem. Soc.* **2012**, *134*, 6388-400.
44. Busby, E.; Xia, J.; Wu, Q.; Low, J. Z.; Song, R.; Miller, J. R.; Zhu, X. Y.; Campos, L. M.; Sfeir, M. Y., A Design Strategy for Intramolecular Singlet Fission Mediated by Charge-Transfer States in Donor-Acceptor Organic Materials. *Nat. Mater.* **2015**, *14*, 426-33.
45. Shushin, A. I., Manifestation of T-Exciton Migration in the Kinetics of Singlet Fission in Organic Semiconductors. *Chem. Phys. Lett.* **2017**, *678*, 283-288.
46. Yong, C. K., et al., The Entangled Triplet Pair State in Acene and Heteroacene Materials. *Nat. Commun.* **2017**, *8*, 15953.